Analysis of a novel CuCl₂ back contact process for improved stability in CdTe solar cells.

Elisa Artegiani[1], Daniele Menossi[1], Huw Shiel*, Vin Dhanak*, Jonathan D. Major*, Andrea Gasparotto[+], Kai Sun[§], and Alessandro Romeo[2].

LAPS- Laboratory for Photovoltaics and Solid State Physics, Department of Computer Science, University of Verona, Ca' Vignal 1, Strada Le Grazie 15, 37134 Verona, Italy, ph.:+39-045-8027974, e-mail address: alessandro.romeo@univr.it

*Stephenson Institute for Renewable Energy and Department of Physics, University of Liverpool, Liverpool, L69 7ZF, UK

+Department of Physics and Astronomy "G. Galilei", University of Padova, Via F. Marzolo 8, 35131 Padova, Italy

§Department of Materials Science and Engineering University of Michigan, Ann Arbor, Michigan, USA

Abstract

One of the crucial points in the production of CdTe solar cells is the insertion of copper in the back contact and in the absorber. As demonstrated by the top performing devices presented in literature: copper is necessary for high efficiency devices.

However, despite this, copper was found to be a fast diffuser degrading the cell in the long term. Different approaches for limiting this effect have been widely presented from several laboratories, from the preparation of Cu$_x$Te by the controlled evaporation of Cu and Te to the application of ZnTe, which incorporates Cu, blocking its diffusion in the bulk.

We have developed a wet deposition method for inserting in the CdTe structure a quantity of copper equivalent to a 0.1 nm thick Cu layer. We are able to reach similar efficiencies to the ones of devices with a standard 2 nm thick evaporated copper layer, but with a dramatic improvement in performance stability.

Keywords: CdTe; CuCl₂; Copper; Back contact

1. Introduction

CdTe and CIGS solar cells, with their respective records of 22.1 % and 22.9 %, have both reached efficiencies near to the 22.3% of multicrystalline silicon [1].
Thin film technology comprises ~5% of the world market, with CdTe modules accounting for around half of this [2]. Polycrystalline CdTe devices are partly limited by low doping concentrations, primarily due to the lack of a dopant with both high solubility and shallow acceptor

---

[1] The first two authors share the same contribution to the work.

[2] Author for correspondence.

level [3]. One of the ongoing challenges of the technology is to produce a good quality and stable ohmic contact, because of the high CdTe electron affinity [4] .

The standard solution has been the insertion of copper at the back contact, which reduces the Schottky barrier via formation of Cu_xTe_{1-x} phases and increased carrier concentration. This produces a "p+" layer at the near back surface which allows carriers to tunnel through the barrier [5]. The mechanism of Cu doping for CdTe has been widely studied [6][7] [8] and utilized in a variety of manners such as via simple copper evaporation or via inclusion in buffer layers at the back surface [9] [10] [11][12][13].

Whilst there has been some success with copper-free back contacts in the past, delivering efficiencies up to 15% [14] [15], it is generally considered that copper is necessary to attain higher efficiency devices.

The use of copper in CdTe remains problematic however given it is a fast diffuser in CdTe and leads to performance degradation of the cells in the long term. Cu has previously been detected at the CdTe/CdS interface [16], and at the CdS/CdTe junction forming recombination centers and shunt pathways [17]. For this reason different approaches have been applied to stabilize Cu at the back contact: such as the formation of Cu_xTe compounds by CdTe etching and subsequent Cu deposition [9][18], or the use of buffer layers such as As_2Te_3 [19] and Bi_2Te_3 [13] in order to avoid copper diffusion, or the development of a ZnTe:Cu back contact [20].

In this paper we analyze copper inclusion via a $CuCl_2$-Methanol solution. This process allows reduction of the incorporated copper quantity without any loss in performance compared to a standard Cu contacting route and simple depositing evenly over the entire area of the sample. Use of a chloride compound was chosen due to the well-known chlorine related benefits of recrystallization, grain growth [21][22][23], and p-type doping (bicomplexes with native defects) [21][24] in CdTe. There is evidence that similar processes have been already applied in some laboratories but without a study of the process' effect [25][26][27][28][29].

Beach et al. suggested that the defects induced by $CdCl_2$, probably Cl-induced donor, increased the solubility of the Cu at Cd substitutional sites impurities Cu^-_{Cd}, which are considered acceptors [30]. The $CuCl_2$ is applied after the standard $CdCl_2$ activation treatment since combining activation treatment and copper doping in a single step is not possible: $CdCl_2$ activation treatment is applied at a temperature which would cause a very large Cu diffusion.

The results of this copper chloride wet deposition method (CCWD) on CdTe are the following:

i) Less Cu required to achieve peak performance: with amount of copper solution which is the equivalent of a 0.1 nm thick evaporated layer, JV characteristic shows a good ohmic back contact without roll over.

ii) Scalable deposition process where copper content can be easily controlled by tuning its concentration in methanol solution.

iii) Improved stability: proved by accelerated aging tests performed at an illumination of one sun and at a temperature of 80°C.

2. Materials and instruments

Current density-voltage (JV) characteristics were measured with a Keithley Source Meter 2420, using a halogen lamp calibrated with a silicon solar cell under an irradiation of 100 mW/cm^2 (AM 1.5).

Drive level capacitance profiling (DLCP), capacitance voltage (CV) and admittance spectroscopy (AS) are carried out by a HP4284A LCR. The temperature is controlled by a Janis cryostat with Lakeshore 325 temperature controller in a vacuum of 10^{-4} Pa and in a range between 100 K and 320 K.

The external quantum efficiency (EQE) was obtained using a commercial LOANA solar cell analysis system, calibrated with a silicon reference sample with known EQE using an incident spotlight of 1 mm x 2 mm area.

The crystalline structure and the compositional phases were analysed by X-Ray diffraction (XRD) with a Philips vertical diffractometer with Cu-Kα radiation, and Goebel monochromator. Secondary ion mass spectrometry (SIMS) depth profiles were obtained on a CAMECA IMS-4 f using an O_2^+ primary ion beam at a 12.5 kV accelerating voltage (corresponding to 8 keV impact energy) and detection of positive secondary ions. A mass resolution m/Δm ≈4000 was employed in the spectrometer to avoid mass interference between the $^{63}Cu^+$ and the $^{126}Te^+$ signals.

X-ray photoelectron spectroscopy (XPS) experiments were performed in a standard ultrahigh vacuum surface science chamber operating at a base pressure of $2 * 10^{-10}$ mbar. Core-level electronic structure was probed using a dual anode Mg Kα (1253.6 eV) X-ray source operating at 200 W and a hemispherical PSP Vacuum Technology electron energy analyser. The spectrometer was calibrated using Au $4f_{7/2}$ at 83.9 eV and has an overall resolution of 0.7 eV. XPS spectra were fitted using Voigt functions after Shirley background removal.

For tunneling electron microscopy-energy dispersive x-ray (TEM-EDX) analysis a JEOL 2100F microscope with CEOS probe corrector was used that was operated in scanning transmission electron microscopy (STEM) mode to acquire simultaneous high angle annular dark-field (HAADF) images, i.e. Z-contrast images, together with EDX element maps. A focused ion beam (FIB) in-situ lift-out method was used for cross-sectional TEM specimen preparation.

3. Device fabrication

CdTe thin film solar cells are made in superstrate configuration by a low-temperature fabrication process based on vacuum evaporation (VE). A 100 nm thick CdS thin film is deposited at 150 °C on an ITO/ZnO 3x3 cm^2 coated soda lime glass and subsequently annealed in vacuum at 450 °C. Then a 7 μm thick CdTe layer is deposited in the same vacuum chamber. The stack is activated by the CdCl$_2$ treatment, consisting of deposition which is applied by wet deposition, and annealed in air at 380 °C.

Prior to the back contact deposition, the CdTe surface is etched by a bromine/methanol solution in order to remove CdCl$_2$ residues and to generate a Te-enriched layer and allow the formation of a Cu$_x$Te compound.

In our standard process, back contact is made by thermal evaporation of a 2.0 nm thick copper layer followed by a 30 nm thick gold layer; annealing in air at 200°C of the finished device is needed to reach good efficiencies.

The CCWD process for CdTe consists of depositing on top of the CdTe layer a solution made of CuCl$_2$ powder diluted in methanol, typically 0.1 g of CuCl$_2$ per litre of methanol. An annealing of

the stack at 200 °C for 30 minutes is applied to allow a chemical reaction between the bulk and the solution. Finally a 30 nm thick gold contact is deposited on free back surface.

In order to compare the CCWD with the VE process, we have deposited on top of the CdTe surface an amount of $CuCl_2$ solution, which is equivalent to a copper layer with a thickness of 0.1 nm. This has been calculated by comparing the amount of copper in the laid out solution with the value obtained by multiplying the copper volume of the thin evaporated layer by its density.

Practically 0.4726 µg of copper have been deposited on an area of 4.5 cm^2 of a 7 µm thick CdTe. Calculating the amount of copper atoms from its atomic mass we have about $1 * 10^{15}$ atoms /cm^2 near to the $0.8 * 10^{15}$ atoms/cm^2 indicated by Kranz et al. [8].

4. Results

4.1 Performance of the devices

A large number of samples have been fabricated with CCWD step process, where the amount of used solution ranged from 10 to 20 µl (pure methanol is also added to improve uniformity) while annealing temperature was optimized at 200°C. Also, optimization of both $CdCl_2$ treatment and CCWD step were done together in order to achieve the best combination in terms of performance. In this way more than 50 samples, with 10 solar cells each of 0.13 cm^2 were produced with the new step process.

These devices have been compared with samples using either a 2 nm or 0.1 nm VE-Cu contacting process. This last one has a very similar copper quantity of the CCWD cells, but deposited by vacuum evaporation and without chlorine. In order to avoid the performance degradation effects due to copper diffusion, one option could be to minimise the amount of copper applied, but this would reduce the performance, due to lower CdTe doping and to a higher back contact barrier.

Figure 1 shows J-V characteristics of three of our best devices obtained inserting copper by evaporation and by wet deposition. Clearly, reducing the amount of evaporated copper from 2 to 0.1 nm, the conversion efficiencies reduce as expected (see Table I). The reduction is mainly caused by a fill factor (FF) loss concurrent to a pronounced rollover.

On the other hand, if the equivalent of 0.1 nm thick copper layer is inserted by CCWD on the CdTe, the series resistance is reduced and fill factor largely increases and conversion efficiencies are comparable to the ones of devices with 2 nm thick back contact layer.

This is quite interesting because it proves that a very small amount of copper (see section 3) is sufficient for CdTe doping as reported by Kranz et al. [8]. However it is very important how and where the Cu is blended in the CdTe matrix, avoiding agglomeration at grain boundaries.

Looking at table II, the average performance parameters show that samples containing a 0.1 nm thick copper layer deposited by CCWD reach almost the same average efficiency (η) than samples containing a 2.0 nm thick copper layer deposited by vacuum evaporation (VE-Cu). In particular the average fill factor of CCWD samples is slightly larger which is quite surprising considering the small amount of Cu.

The choice of $CuCl_2$ as Cu carrier has been done according to the well-known effects of chlorine-based treatments, enhancing a chemical reaction with CdTe [31], generating a rearrangement of the CdTe structure and reducing the grain boundaries' effect. However, the results show that inserting

copper by chlorine carrier improves the back contact, but it can not be excluded that it also might change the interface and the bulk structure of the absorber.

In order to clarify this aspect, an analysis of the spectral response of two different cells, with efficiencies around 13%, have been pursued by External Quantum Efficiency measurements, performed on CCWD and VE-Cu samples. EQE responses of the different cells do not show significant differences, attesting that CCWD does not influence band gap or carrier lifetime. Similar response for different cells at long-wavelength region show that the CdS_xTe_{1-x} intermixed layer has not been modified by the additional chlorine treatment; as it is known that the formation of an intermixed layer reduces the band gap [32], shifting the EQE response.

4.2 Structural analysis

The activation treatment, with $CdCl_2$, is typically changing the grain structure of the absorber, in particular is affecting both shape (and size in case of low temperature deposited CdTe) and orientation of the grains [33].

Thus it is interesting to verify if CCWD process would also modify the structure of the CdTe bulk, due to the presence of chlorine. For this reason, XRD patterns have been acquired on the surface of the completed VE-Cu and CCWD photovoltaic devices (see figure 2), considering that in the standard geometry the x-rays are able to penetrate more than 0.5 μm in the stack.

As shown in figure 2, CdTe peaks are present in both samples, as expected.

Moreover we can observe a slightly different recrystallization for the CCWD case, where the preferential orientation of the (111) peak is completely lost in favour of the (422) orientation. In particular for the VE-Cu case (111)>(311) and (442) while for the CCWD case (442)>(311)>(111). This shows that copper chlorine introduces copper in the bulk of CdTe by changing its structure, affecting the orientation of the grains. Also AFM pictures show a slightly different grain structure, as depicted in figure 3.

4.3 Doping and identification of defects

A very important aspect is understanding the effects of the different copper insertion processes in the CdTe doping. As already mentioned, a reduced Cu quantity would suggest a lower CdTe doping, but this appears to be in contrast with the devices performances, which in the case of CCWD samples does not suffer of any Cu deficiency. With capacitance voltage (CV) and drive level capacitance profiling (DLCP) measurements on VE-Cu and CCWD samples the net charge density in CdTe of acceptor-minus-donor states can be estimated as a function of distance from the junction. The CV profiles (indicated in figure 4 with open dots) show the contribution of both deep and shallow defects, while the deepest states hardly affect the DLCP curves (full dots), so the difference between each pair of curves is associated to the presence of deep states [34].

At 1 MHz, the net charge density profile of the VE-Cu sample (see figure 4, graph on the right) is much more temperature dependent than the $CuCl_2$ one: as the temperature rises, in the VE-Cu case (fig.4, right side) the net charge density increases constantly with temperature, while in CCWD case (fig.4 left side) the main increase happens only between 240 K and 270 K. This suggests that the dominant defects are of different nature in the two samples, though both types of samples show the presence of deep defects. The net charge density is determined from the lower part of the U-shape

profile in order to avoid effects due to others factors, such as a not perfectly ohmic back contact or the limited thickness of CdTe [35]. At 300 K the VE-Cu sample show a little higher net charge density than the CCWD case: $2 * 10^{14}$ cm^{-3} versus $1.5 * 10^{14}$ cm^{-3}. At 210 K the net charge density of VE-Cu sample drops at $3 * 10^{13}$ cm^{-3} while it stays at $6 * 10^{14}$ cm^{-3} for the CCWD case, in the first case we can conclude that some defects freeze out. Again in figure 4, the profiles referred to the VE-Cu case increase in the right part of the graph; this effect is influenced by the back contact, revealing that the depletion region extends too close to the contact.

Similar analysis has been done also at lower frequencies such as 10 kHz (see figure 5) : in the VE-Cu case, we can imagine that some defects are slower and/or more distant from the valence band [34] compared to that of the CCWD case. The defects in the VE-Cu type are following the voltage signal at high temperature or at low frequency: so that at 10 kHz the net charge density is $3 * 10^{14}$ cm^{-3}. On the other hand for the CCWD sample the net charge density stays stable at $1.5 * 10^{14}$ cm^{-3}. Since the samples, except for the copper deposition step, have similar fabrication process, we can conclude that the CuCl$_2$ treatment results to different defects in the CdTe.

However the overall net charge density is very close for the two processes. Thus it can be concluded that CdTe has similar level of doping with a reduced amount of Cu, if introduced with chlorine carrier, compared to the 2 nm thick copper layer deposited by evaporation.

In order to identify the nature of the different defects seen by CV-DLCP measurements and to understand what happens when copper is introduced in CdTe bounded to chlorine, admittance spectroscopy analysis were performed on VE-Cu and CuCl$_2$ samples. AS measurements allow to estimate the activation energy (E_a) and cross section (σ_a) of the dominant traps above the valence band and identify the nature of the defects (see figure 6 and table III).

Both samples show the presence of defect A, identified as the $V_{Cd} – Cl_{Te}$ complex, usually called A center [24]. However they show also different deep defects: in the CuCl$_2$ sample two defects (B) are detected: with E_a between 0.34 eV and 0.37 eV above the valence band, in this range the defects are attributed to the Cu at Cd substitutional sites impurities Cu$^-_{Cd}$ [30][36]. These were also detected by Beach et al.: they reported that the concentration of these defects was higher in CdCl$_2$ treated samples, implying that the defects induced by CdCl$_2$ (probably Cl-induced donor) increased the solubility of Cu$^-_{Cd}$ [30].

In this paper all the samples are CdCl$_2$ treated, however by detecting these defects only for the CuCl$_2$ sample suggests that Cl presence increases the Cu solubility into the CdTe bulk. Moreover, by reducing the amount of copper the number of interstitial copper defects Cu$_i$ is also reduced. It has been reported that the Cu substitution in Cd vacancy Cu$^-_{Cd}$ acts as an acceptor, by increasing the p-type doping, while the interstitial copper Cu$_i$ is a shallow donor, which compensate the doping [37][30] [36]. For this reason the formation of the Cu$^-_{Cd}$ defects is desirable.

On the other hand, Cu$^-_{Cd}$ levels are not measured in the VE-Cu sample, despite the higher copper concentration. However this shows that this type of defect is not dominant in the VE-Cu sample. In this case, due to the large amount of copper, Cu$^-_{Cd}$ and Cu$_i$ are compensated.

The VE-Cu sample shows two deeper dominant defects (C) in the range of 0.43 – 0.45 eV above the valence band, usually detected in our standard samples [18][38], which are not clearly attributed. Beach et al. [30] as well as Wei et al. [39] consider plausible to assign these values to the U-center Te$^{2-}_i$: a deep acceptor level. Also, Beach et al. highlight that these defects have a higher density for CdCl$_2$ treated samples, implying that CdCl$_2$ contributes to their formation, this has been previously observed also in our samples [38].

4.4. Analysis of the diffusion of copper element

Figure 7 shows HAADF images together with corresponding EDX Cu maps on $CuCl_2$ and VE-Cu devices. The two EDX maps are not normalized and for this reason they cannot be compared in absolute values (i.e. signal intensity), however our aim here is to analyse the distribution of the copper in each sample.

In both samples, copper is distributed throughout the CdTe layer, including the back contact region. Nevertheless, in the picture for the first case the magenta colour is almost homogeneously distributed while for the second case it is concentrated at the back. This means a larger uniformity of copper for the VE-Cu case (top), as a larger content of magenta colour is observable all over the CdTe bulk. On the other hand, the CCWD case shows a strong difference in the copper distribution: a higher contrast is observed near the back contact.

This suggests that in the $CuCl_2$ sample a larger amount of copper is fixed at the back contact despite it is 1/20 of the evaporated copper (see section 3). The fact that most of the copper is kept at the contact explains the lower back contact barrier in the $CuCl_2$ sample and so the high fill factor value. In order to check and confirm this observed different rate of copper diffusion, SIMS depth profiles have been analysed in the VE-Cu and the CCWD samples; both samples were coated with a 25 nm thick gold layer.

The SIMS profiles (shown in figure 8) confirm the highest amount of copper on the surface for the VE-Cu case. The Cu, in this case, diffuses into the gold layer, so near the surface a large amount of Cu is registered. So when we have to compare the two different samples, for VE-Cu we should consider the amount measured at a depth of 30 nm, value where the copper presence starts in the CCWD sample.

Moreover in the VE-Cu sample there is a large copper diffusion in the first 400 nm (in depth), over this value the signal reduces at the limit of the sensitivity of the instrument. For the CCWD sample the signal decreases to the sensitivity limit within 200 nm; moreover the copper amount in this region is lower than in the VE-Cu sample. Finally, in the VE-Cu sample, we can observe copper diffusion inside the gold layer, due to the annealing of the finished back contact.

4.5 Back surface analysis.

Although the copper distribution in the CdTe varied dependent on the application method, it is useful to determine if it stays in elemental form or if it generates different compounds on the CdTe surface. For this purpose XPS characterization has been performed on the surface of VE-Cu and CCWD samples; both samples were prepared with only 5 nm thick gold layer on top, in order to allow the analysis.

In figure 9, the XPS Te 3d core levels show that while in the $CuCl_2$ sample Te-O and Te/Te-Cd peaks have comparable heights, in the VE-Cu sample the Te-O peaks are much more intense than the Te/Te-Cd ones. Han et al. [40], reported a same increase of the Te-O peak and decrease of the Te/Te-Cd peak when leaving the CdTe sample exposed to air. So we can conclude that in the VE-Cu sample the Te layer is mainly oxidized, while for the CCWD case Te-O and elemental Te/Te-Cd have similar signals, thus the CCWD sample shows a larger presence of Te in the back contact region. This can explain the improved performance of the back contact for CCWD case (no rollover

in the J-V curve is observed). A Te layer is widely used as a buffer to improve the back contact because of its high valence band maximum, which is around 5.40-5.45 eV and stays at intermediate levels between the CdTe valence-band maximum (5.8 eV) below the vacuum level and the gold work function (5.1 eV). It reduces the CdTe back contact barrier [41].

Very important is that despite the lower Cu amount for the CCWD case, this sample shows high Te-Cd peaks. Thus in this case at the back contact it is placed a larger amount of copper (as supported by the already shown EDX mapping during TEM analysis). Moreover, an XPS study on Cu-free CdTe was made for reference. The change in separation between the two main peaks (Te-Cd and Te-O bonding) supports the presence of the Te-Cu component.

From this analysis, we can conclude that depositing $CuCl_2$ on a Te rich layer (generated by the Br-MeOH etching), the Te binds with Cu during the annealing step oxidizing to a very limited extent. This is another part of the jigsaw that explains the higher performance of the back contact, since Cu_xTe buffer binds Cu and reduces its diffusion in the bulk as shown by Wu et al. [9]. This buffer can also be generated by depositing copper on the bromine-methanol etched CdTe surface as shown by Rimmaudo et al. [18] .

5. Discussion and Performance stability of the cells.

At this stage we have acquired that $CuCl_2$ step process is able to provide a performing back contact with a minimum amount of copper.

XPS, SIMS and EDX analyses confirm that a large amount of Cu is concentrated and fixed very near to the back contact suggesting a superior stability of the finished devices.

The best way to analyse and verify the performance degradation of the solar cells according to the different process discussed here, it is to apply accelerated stress tests (AST) on the photovoltaic devices. In a specific metal chamber, where a rack of halogen lamps and a temperature-controlled system allows to keep the cells under an illumination of around 1000 W/m^2 and at a temperature of 80°C, the cells are positioned for a time up to 1000 hours and their conversion efficiency measured every 300 hours.

Two different sets of solar cells were positioned in the AST box, one with VE-Cu samples and one with CCWD samples; both exhibited an average efficiency of about 14 % prior to aging. Their performance degradation has been analyzed by measuring their efficiencies at different time steps. As it can be seen in the graph on the left of figure 10 and on table IV, the CCWD samples show a reduced degradation. In particular, after 1008 hours of aging they have an average efficiency of (10.6 ± 0.4) % compared to the (7.3 ± 0.4) % of the Cu samples. The cells show their major efficiency drop during the first period of aging, and also just after 336 hours the average efficiency discrepancy is clear: (11.5 ± 0.4) % versus (8.1 ± 0.3) %.

The different level of degradation depends mainly on the FF: after 1008 hours, setting to 100 the initial values, the average FF of CCWD samples is reduced to 85% of its initial value, the average Voc to 90%, and the average Jsc to 99%. On the contrary, the VE-Cu samples have reduced their average FF to 69%, their average Voc to 82%, and their average Jsc to 95%.

After the complete AST cycle the CCWD samples exhibit 76% of the initial average conversion efficiency, while the efficiencies of the VE-Cu samples are halved.

The higher stability of CCWD-CdTe devices compared to the VE-Cu ones, as expected from the characterizations that have been discussed above, is confirmed. The extremely reduced amount of

Cu (more than 20 times less) in the CCWD device also contributes to this stability. Diffusion is proportional to concentration, the amount of Cu which diffuses into the CdTe layer is regulated by its concentration gradient in the absorber film.

When large Cu amount is diffused, it can lead to shunt paths, reflecting in reduced FF as observed in this paper. So according to this argument, more Cu delivers increased migration towards the p-n junction. This hypothesis has been also partly confirmed by additional CV-DLCP characterizations, which were made on VE-Cu and CCWD samples after 336 h AST, where the main drop in efficiency value is occurred.

By comparing these profiles (shown in figure 11) with the pre-aging profiles depicted in figure 4, we can interpret the mechanisms of efficiency degradation. The net charge density of the CCWD sample drops from $1.5 * 10^{14}$ cm^{-3} to $5 * 10^{13}$ cm^{-3} after aging, and similarly the one of the VE-Cu sample, from $2 * 10^{14}$ cm^{-3} to $4 * 10^{13}$ cm^{-3}. More interesting, for VE-Cu case, the net charge density measured at lower temperatures (also shown in fig.4) is low and the profiles are influenced by back contact effects (i.e. the depletion region extends too close to the back contact). As Cu increases, the extension of the depletion region widens to the metal back contact. This trend is stronger with time and can explain the reason of the larger reduction in performance of solar cells contacted with a 2.0 nm thick Cu layer. A higher amount of copper diffusion from the back contact could lead to the formation of a larger amount of compensating defects. As also suggested by other groups, an excessive copper diffusion can compensate the Cu$_{Cd}^-$ acceptors with Cu$_i$ donors [8][37]. Therefore the smaller amount of Cu needed with the CuCl$_2$ copper deposition method leads to a reduced formation of compensating defects, and thus to the fabrication of more stable samples.

6. Conclusions

A wet deposition method has been developed in order to insert copper at the back contact of CdTe solar cells. Using a solution allows to simply deposit any ideal small amount of copper evenly over the entire area of the sample. In particular a copper chloride solution has been used because of the well-known effects of chlorine on CdTe such as recrystallization, grain growth [21], and possibly p-type doping [21][24].

The samples exhibit a good ohmic back contact without rollover and with efficiencies comparable to those of samples, which are vacuum coated but with an amount of Cu twenty times larger. Moreover, a significant stability improvement has been achieved, as attested by the accelerated aging tests performed at an illumination of one sun and at a temperature of 80°C.

We have detected that the CuCl$_2$ treatment affects both bulk and back contact of the CdTe.

1. Bulk

CV-DLCP profiles of VE-Cu and CCWD samples reveal the presence of different dominant defects. Only for the CCWD sample the dominant defects, identified by AS, are in a range of energies that have been attributed to the substitutional Cu impurities Cu$_{Cd}^-$ [30,36], known as acceptors in CdTe. Since all the different samples have been CdCl$_2$ treated, but only CuCl$_2$ treated samples show this type of defects, it can be supposed that the introduction of copper bounded to chlorine helps the solubility of the Cu$_{Cd}^-$ acceptors since chlorine increases their solubility [30]. As a consequence, the p-type doping of CdTe is improved [8,41]. At low temperatures CV/DLCP show that VE-Cu samples are strongly influenced by back contact effects, their depletion region extends

closer to the back contact, and thus the net charge density is low. This effect appears mainly at the lowest temperatures, suggesting the presence of shallow donors, exactly as Cu_i, that, being closer to the band, have faster response at low temperatures than deep defects such as the Cu^-_{Cd} [34]. This effect increases with aging time, due to copper diffusion and consequent formation of Cu_i donors.

2. Back contact

Moreover, TEM images show for CCWD samples a larger inhomogeneity in copper distribution from the back contact to the junction, implying that the copper stays fixed at the back contact. XPS spectra explain how the copper is fixed: in spite of the reducing copper quantity, the CCWD sample reveals a large presence of Te-Cu peaks, demonstrating that a Cu_xTe compound is formed stabilizing Cu at the back contact [9].

Compared to VE-Cu the CCWD process generates more tellurium and less tellurium oxides, which is beneficial to the cell performance as Te layer is widely used as buffer to reduce the CdTe back contact barrier [41]. The improved back contact stability, given by the Cu-Te compounds, is supported by the reduced copper diffusion towards the CdTe/CdS junction; this has been confirmed by SIMS depth profiles.

Finally AST analysis has shown a different degradation of the solar cell devices according to the Cu inclusion method. For VE-Cu solar cells the degradation in performance is mainly due to the FF reduction. While for the CCWD cells, the degradation is very much limited.

In conclusion the $CuCl_2$ wet deposition process is a simple and advantageous method to insert copper in the back contact of CdTe solar cells. It allows the formation of Cu^-_{Cd} acceptor defects, reducing the formation of the compensating donors Cu_i.

In the light of the results obtained, the conclusion is that this process step improves the lifetime of CdTe devices, without efficiency losses.

1. Green, M.A., Hishikawa, Y., Dunlop, E.D., Levi, D.H., Hohl-Ebinger, J., and Ho-Baillie, A.W.Y. (2018) Solar cell efficiency tables (version 52). *Prog. Photovoltaics Res. Appl.*, **26** (7), 427–436.

2. Philips, D.S., and Warmuth, W. (2019) Photovoltaics Report 2019. *Fraunhofer ISE*, (March), 1–43.

3. Wei, S.H., and Zhang, S.B. (2002) Chemical trends of defect formation and doping limit in II-VI semiconductors: The case of CdTe. *Phys. Rev. B - Condens. Matter Mater. Phys.*, **66** (15), 1–10.

4. Demtsu, S.H., and Sites, J.R. (2006) Effect of back-contact barrier on thin-film CdTe solar cells. *Thin Solid Films*, **510** (1–2), 320–324.

5. Corwine, C.R., Pudov, A.O., Gloeckler, M., Demtsu, S.H., and Sites, J.R. (2004) Copper

inclusion and migration from the back contact in CdTe solar cells. *Sol. Energy Mater. Sol. Cells*, **82** (4), 481–489.

6. Das, S.K., and Morris, G.C. (1992) Influence of growth and microstructure of electrodeposited cadmium telluride films on the properties of n-CdS/p-CdTe thin-film solar cells. *J. Appl. Phys.*, **72** (10), 4940–4945.

7. Kučys, E., Jerhot, J., Bertulis, K., and Bariss, V. (1980) Copper impurity behaviour in CdTe films. *Phys. Status Solidi*, **59** (1), 91–99.

8. Kranz, L., Gretener, C., Perrenoud, J., Schmitt, R., Pianezzi, F., La Mattina, F., Blösch, P., Cheah, E., Chirilă, A., Fella, C.M., Hagendorfer, H., Jäger, T., Nishiwaki, S., Uhl, A.R., Buecheler, S., and Tiwari, A.N. (2013) Doping of polycrystalline CdTe for high-efficiency solar cells on flexible metal foil. *Nat Commun*, **4**.

9. Wu, X., Zhou, J., Duda, a., Yan, Y., Teeter, G., Asher, S., Metzger, W.K., Demtsu, S., Wei, S.-H., and Noufi, R. (2007) Phase control of CuxTe film and its effects on CdS/CdTe solar cell. *Thin Solid Films*, **515** (15), 5798–5803.

10. Gessert, T.A., Asher, S., Johnston, S., Duda, A., Young, M.R., and Moriarty, T. (2006) Formation Of ZnTe: Cu/Ti Contacts at High Temperature for CdS/CdTe Devices. *Conf. Rec. 2006 IEEE 4th World Conf. Photovolt. Energy Conversion,* 432–435.

11. Li, J., Diercks, D.R., Ohno, T.R., Warren, C.W., Lonergan, M.C., Beach, J.D., and Wolden, C.A. (2015) Controlled activation of ZnTe:Cu contacted CdTe solar cells using rapid thermal processing. *Sol. Energy Mater. Sol. Cells*, **133**, 208–215.

12. Romeo, N., Bosio, A., Mazzamuto, S., Romeo, A., and Vaillant Roca, L. (2007) High Efficiency CdTe/CdS Thin Film Solar Cells with a Novel Back Contact. *Proc. 22nd Eur. Photovolt. Sol. Energy Conf.*, 1919–1921.

13. Romeo, A., Salavei, A., Rimmaudo, I., Bosio, A., Menossi, D., Picinelli, F., and Romeo, N. (2013) Electrical characterization and aging of CdTe thin film solar cells with Bi2Te3 back contact. *Conf. Rec. 39th IEEE Photovolt. Spec. Conf.*, 1178–1182.

14. Romeo, N., Bosio, a., and Romeo, a. (2010) An innovative process suitable to produce high-efficiency CdTe/CdS thin-film modules. *Sol. Energy Mater. Sol. Cells*, **94** (1), 2–7.

15. Bätzner, D.L., Romeo, A., Zogg, H., Wendt, R., and Tiwari, A.N. (2001) Development of efficient and stable back contacts on CdTe/CdS solar cells. *Thin Solid Films*, **387** (1–2), 151–154.

16. Grecu, D., and Compaan, a. D. (1999) Photoluminescence study of Cu diffusion and electromigration in CdTe. *Appl. Phys. Lett.*, **75** (1999), 361.

17. Dobson, K.D., Visoly-fisher, I., Hodes, G., and Cahen, D. (2000) Stability of CdTe / CdS thin-film solar cells. *Sol. Energy Mater. Sol. Cells*, **62**, 295–325.

18. Rimmaudo, I., Salavei, A., Artegiani, E., Menossi, D., Giarola, M., Mariotto, G., Gasparotto, A., and Romeo, A. (2017) Improved stability of CdTe solar cells by absorber surface etching. *Sol. Energy Mater. Sol. Cells*, **162** (December 2016), 127–133.

19. Romeo, N., Bosio, A., and Romeo, A. (2010) An innovative process suitable to produce high-efficiency CdTe/CdS thin-film modules. *Sol. Energy Mater. Sol. Cells*, **94** (1), 2–7.

20. Gessert, T.A., Mason, A.R., Sheldon, P., Swartzlander, A.B., Niles, D., and Coutts, T.J. (1996) Development of Cu- doped ZnTe as a back- contact interface layer for thin- film CdS/CdTe solar cells. *J. Vac. Sci. Technol. A Vacuum, Surfaces, Film.*, **14** (3), 806–812.

21. Dharmadasa, I. (2014) Review of the CdCl2 Treatment Used in CdS/CdTe Thin Film Solar Cell Development and New Evidence towards Improved Understanding. *Coatings*, **4** (2), 282–307.

22. Major, J.D., Treharne, R.E., Phillips, L.J., and Durose, K. (2014) A low-cost non-toxic post-growth activation step for CdTe solar cells. *Nature*, **511** (7509), 334–337.

23. Salavei, A., Rimmaudo, I., Piccinelli, F., Menossi, D., Bosio, A., Romeo, N., and Romeo, A. (2014) Analysis of CdTe activation treatment with a novel approach. *28th Eur. Photovolt. Sol. Energy Conf. Exhib.*, 2140–2142.

24. Castaldini, A., Cavallini, A., Fraboni, B., Fernandez, P., and Piqueras, J. (1996) Comparison of electrical and luminescence data for the A center in CdTe. *Appl. Phys. Lett.*, **69** (23), 3510–3512.

25. Mao, D., Blatz, G., Wickersham, C.E., and Gloeckler, M. (2016) Correlative impurity distribution analysis in cadmium telluride (CdTe) thin-film solar cells by ToF-SIMS 2D imaging. *Sol. Energy Mater. Sol. Cells*, **157**, 65–73.

26. Aris, K.A., Rahman, K.S., Enam, F.M.T., Kamaruzzaman, M.I. Bin, Yahya, I. Bin, and Amin, N. (2016) An investigation on copper doping to CdTe absorber layers in CdTe thin film solar cells. *2016 Int. Conf. Adv. Electr. Electron. Syst. Eng.*, 405–408.

27. Gordillo, G., Grizalez, M., Moreno, L.C., and Landazábal, F. (2000) Influence of the optical window on the performance of TCO/CdS/CdTe solar cells. *Phys. Status Solidi Basic Res.*, **220** (1), 215–219.

28. Munshi, A.H., Kephart, J.M., Abbas, A., Danielson, A., Gélinas, G., Beaudry, J.N., Barth, Walls, J.M., and Sampath, W.S. (2018) Effect of CdCl2 passivation treatment on microstructure and performance of CdSeTe/CdTe thin-film photovoltaic devices. *Sol. Energy Mater. Sol. Cells*, **186** (June), 259–265.

29. Munshi, A.H., Kephart, J., Abbas, A., Raguse, J., Beaudry, J., Barth, K., Sites, J., Walls, J., and Sampath, W. (2018) Polycrystalline CdSeTe/CdTe Absorber Cells With 28 mA/cm^2 Short-Circuit Current. *IEEE J. Photovoltaics*, **8** (1), 310–314.

30. Beach, J., Seymour, F.H., Kaydanov, V.I., and Ohno, T.R. (2006) Studies of Basic Electronic Properties of CdTe-Based Solar Cells and Their Evolution During Processing and Stress. *Subcontract Rep. NREL/SR-520-41097*, (January).

31. McCandless, B.E. (2001) Thermochemical and Kinetic Aspects of Cadmium Telluride Solar Cell Processing. *Proc. 2001 MRS Spring Meet.*, H1.6, 1-12.

32. Yan, Y., Dhere, R.G., Jones, K.M., and Al-Jassim, M.M. (2001) Influence of substrate structure on the growth of CdTe thin films. *J. Appl. Phys.*, **89** (11 I), 5944–5948.

33. Bosio, A., Romeo, A., Menossi, D., Mazzamuto, S., and Romeo, N. (2011) Review: The second-generation of CdTe and CuInGaSe2 thin filmPV modules. *Cryst. Res. Technol.*, **46**, 857–864.

34. Heath, J.T., Cohen, J.D., and Shafarman, W.N. (2004) Bulk and metastable defects in CuIn1−xGaxSe2 thin films using drive-level capacitance profiling. *J. Appl. Phys.*, **95** (3), 1000–1010.

35. Li, J. V., Halverson, A.F., Sulima, O. V., Bansal, S., Burst, J.M., Barnes, T.M., Gessert, T.A., and Levi, D.H. (2012) Theoretical analysis of effects of deep level, back contact, and absorber thickness on capacitance-voltage profiling of CdTe thin-film solar cells. *Sol. Energy Mater. Sol. Cells*, **100**, 126–131.

36. Balcioglu, A., Ahrenkiel, R.K., and Hasoon, F. (2000) Deep-level impurities in CdTe/CdS thin-film solar cells. *J. Appl. Phys.*, **88** (12), 7175–7178.

37. Tang, J., Mao, D., Ohno, T.R., Kaydanov, V., and Trefny, J.U. (1997) Properties of ZnTe:Cu thin films and CdS/CdTe/ZnTe solar cells. *Proc. 26th IEEE Photovolt. Spec. Conf.*, 439–442.

38. Rimmaudo, I., Salavei, A., and Romeo, A. (2013) Effects of activation treatment on the electrical properties of low temperature grown CdTe devices. *Thin Solid Films*, **535**, 253–256.

39. Wei, S.-H., Zhang, S.B., and Zunger, A. (2000) First-principles calculation of band offsets, optical bowings, and defects in CdS, CdSe, CdTe, and their alloys. *J. Appl. Phys.*, **87** (2000), 1304.

40. Jun-Feng, H., Liu, X., Li-Mei, C., Hamon, J., and Besland, M.P. (2015) Investigation of oxide layer on CdTe film surface and its effect on the device performance. *Mater. Sci. Semicond. Process.*, **40**, 402–406.

41. Song, T., Moore, A., and Sites, J.R. (2018) Te layer to reduce the CdTe back-contact barrier. *IEEE J. Photovoltaics*, **8** (1), 293–298.

Table I: efficiency parameters of devices of Fig. 1: conversion efficiency (η), fill factor (FF), open circuit voltage (Voc) and short circuit current density (Jsc).

Copper quantity	η (%)	FF (%)	Voc (mV)	Jsc (mA/cm^2)
CCWD	15.9 ± 0.2	73.1 ± 0.5	859 ± 1	25.4 ± 0.1
VE-Cu 2.0 nm	16.1 ± 0.2	72.0 ± 0.5	866 ± 1	$25,8 \pm 0.1$
VE-Cu 0.1 nm	13.8 ± 0.2	66.0 ± 0.5	852 ± 1	24.5 ± 0.1

Table II: average efficiency parameters of devices.

Copper quantity	η (%)	FF (%)	Voc (mV)	Jsc (mA/cm^2)
CCWD	15.7 ± 0.3	71.4 ± 1.4	852 ± 5	25.8 ± 0.3
VE-Cu 2.0 nm	15.9 ± 0.1	71 ± 1.3	852 ± 10	26.4 ± 0.7
VE-Cu 0.1 nm	13.8 ± 0.2	66.2 ± 0.8	847 ± 2	24.6 ± 0.5

Table III: List of defects identified by admittance spectroscopy.

CCWD sample		Attribution	VE-Cu sample	
E_a [meV]	σ_a [cm^{-2}]		E_a [meV]	σ_a [cm^{-2}]
		A	109 ± 3	$1.9 * 10^{-16}$
125 ± 6	$4.6 * 10^{-16}$	A	121 ± 4	$5.5 * 10^{-16}$
136 ± 4	$2.0 * 10^{-15}$	A	134 ± 3	$1.7 * 10^{-15}$
349 ± 5	$2.0 * 10^{-13}$	B		
367 ± 6	$8.2 * 10^{-13}$	B		
		C	445 ± 10	$5.8 * 10^{-12}$
		C	449 ± 9	$1.9 * 10^{-13}$

Table IV: average efficiency parameters of CuCl$_2$ and VE-Cu devices before the aging, and after 1008 hours of AST.

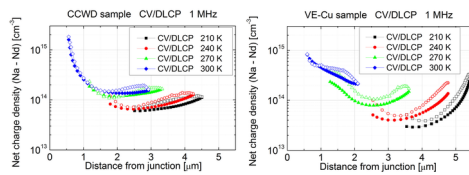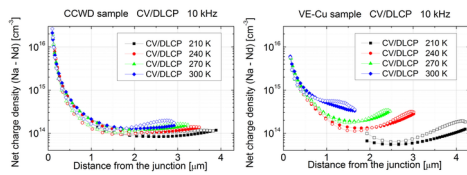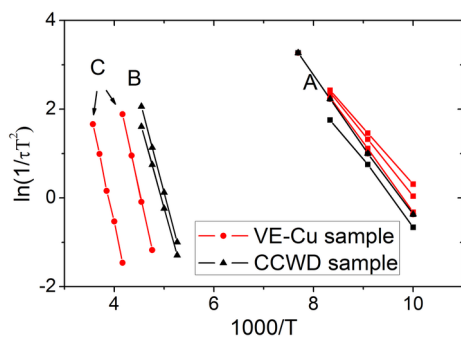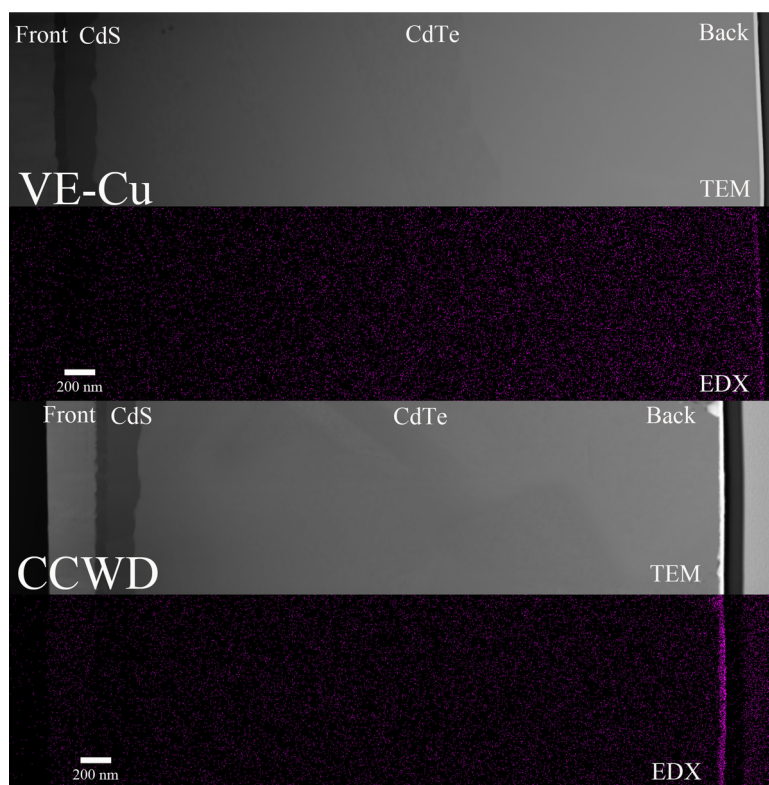| Samples	η (%)	FF (%)	Voc (mV)	Jsc (mA/cm^2)
CuCl$_2$ before aging	13.9 ± 0.3	67 ± 2	845 ± 3	24.5 ± 0.4
CuCl$_2$ after 1008 h of AST	10.6 ± 0.4	57 ± 3	764 ± 4	24.2 ± 0.4
VE-Cu before aging	13.9 ± 0.8	69 ± 4	849 ± 5	23.6 ± 0.2
VE-Cu after 1008 h of AST	7.3 ± 0.4	47 ± 2	694 ± 5	22 ± 1
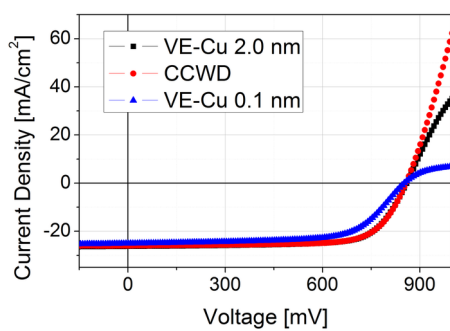
PIP_3148_F1.tif
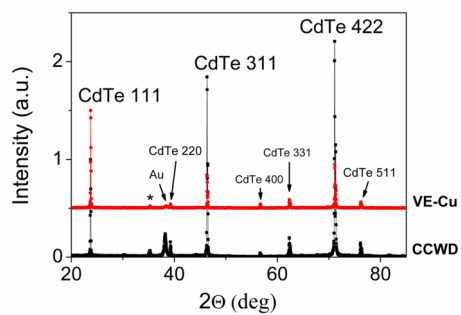
PIP_3148_F2.tif
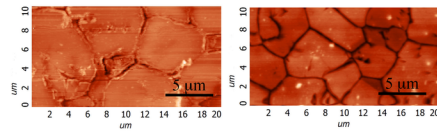
PIP_3148_F3.tif

PIP_3148_F4.tif
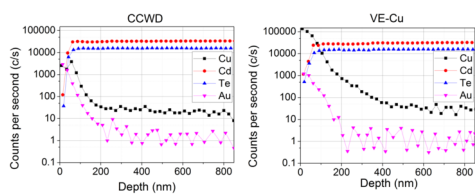
CCWD sample CV/DLCP 10 kHz

VE-Cu sample CV/DLCP 10 kHz
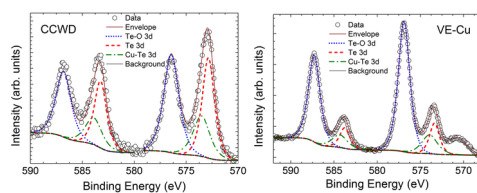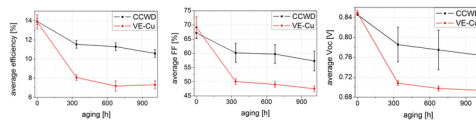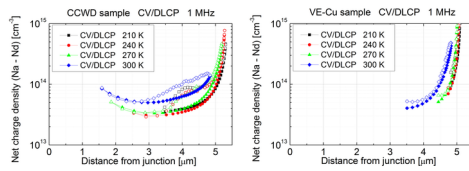
PIP_3148_F5.tif

PIP_3148_F6.tif

PIP_3148_F7.tif

PIP_3148_F8.tif

PIP_3148_F9.tif

PIP_3148_F10.tif

PIP_3148_F11.tif